PDF SIMULATION OF PREMIXED BUNSEN FLAMES

Michael Stöllinger and Stefan Heinz
University of Wyoming, Department of Mathematics
1000 East University Avenue, Laramie, WY 82071, USA
mstoell@uwyo.edu

ABSTRACT

The use of probability density function (PDF) methods for turbulent combustion simulations is very attractive because arbitrary finite-rate chemistry can be exactly taken into account. However, many real flames involve a variety of mixing regimes (non-premixed, partially-premixed and premixed turbulent combustion), and the development of PDF methods for partially-premixed and premixed turbulent combustion turned out to be a very challenging task. The extension of the range of applicability of PDF methods to the fast flamelet chemistry of turbulent premixed flames is shown in this work. It is worth noting that the same methodology can be used in corresponding filter density function (FDF) methods.

INTRODUCTION

The extension of Reynolds-averaged Navier-Stokes (RANS) equations by probability density function (PDF) methods (Pope, 1985; Heinz, 2003) has significant advantages for turbulent reacting flow simulations due to the fact that there is no need to involve approximations of uncertain generality to close chemical reaction rates. The same advantage is given by the generalization of large eddy simulation (LES) methods by filter density function (FDF) methods (Colucci et al., 1998). FDF methods are usually more accurate but also more expensive than PDF methods. Due to the exact treatment of chemical reactions, the performance of PDF and FDF methods is essentially determined by the modeling of the transport of scalars (e.g., species mass fractions and temperature). Such scalar transport models involve two ingredients: a scalar mixing frequency model that determines the characteristic time scale of mixing, and a scalar mixing model that describes the change of the PDF of a scalar (Fox, 2003).

Most of the previous applications of PDF and FDF methods were related to simulations of non-premixed turbulent combustion. In this case, the characteristic length and time scales of scalar fields are usually larger than the characteristic length and time scales of turbulent motions. Correspondingly, the scalar mixing frequency can be assumed to be controlled by the frequency of large-scale turbulent motions. The performance of scalar mixing models for non-premixed turbulent combustion is relatively well investigated. Mitarai et al. (2005) compared predictions of different mixing models to the results of direct numerical simulation (DNS). Merci et al. (2006) and Xu and Pope (2000) studied various scalar mixing models in turbulent natural gas diffusion flames.

Applications of PDF and FDF methods to premixed turbulent combustion are more complicated than calculations of non-premixed turbulent combustion. The appearance of fast flamelet chemistry may result in very thin reaction zones such that scalar mixing can take place on scales which are much smaller than all scales of turbulent motions (Anand and Pope, 1987; Mura et al., 2003). Correspondingly, there exist only a few applications of PDF methods to premixed flames. To overcome problems of earlier approaches, Mura et al. (2003) recently suggested a PDF model where the outer parts of the flame structure (reactants side and products side) are described by a standard scalar mixing model whereas the inner part (the reaction zone) is described by a flamelet model. However, this approach is complicated and related to several questions (e.g. regarding the matching of both combustion regimes). The scalar mixing frequency is provided via a transport equation for the scalar dissipation rate, which is constructed by adding effects of chemical reactions to corresponding equations for non-reacting scalars. The model of Mura et al. (2003) requires the adjustment of six parameters to the flow considered, the modeling of the dissipation rate of non-reacting scalars does not agree with many other models (Sanders and Goekalp, 1998), and there are questions regarding the inclusion of chemical reaction effects. More recently, Lindstedt and Vaos (2006) and Cha and Trouillet (2003) developed models that relate the scalar mixing frequency of reacting scalars to the characteristic frequency of turbulent motions and the scalar mixing frequency of non-reacting scalars, respectively. Both approaches use flamelet ideas in conjunction with several other assumptions: e.g., the assumption of a local equilibrium between production and dissipation, and the assumption of local homogeneity and isotropy.

In this work, we present a new model for the scalar mixing frequency. The model is constructed such that the scalar variance is conserved. Details on the model derivation and characteristic features can be found elsewhere (Stöllinger and Heinz, 2007). The performance of this new model is demonstrated by application to PDF simulations of three turbulent premixed Bunsen flames.

THE FLAMES CONSIDERED

The turbulent premixed F1, F2, and F3 flames studied experimentally by Chen et al. (1996) are considered to investigate the performance of the PDF modeling approach. The three highly stretched stoichiometric methane-air flames cover a range of Reynolds and Damköhler numbers. Based on an order of magnitude analysis Chen et al. (1996) found that all three flames are located in the distributed reaction zones regime. In particular, the F1 flame is located at the borderline to the well stirred reactor regime, and the F3 flame is located at the borderline to the flamelet regime. Due to the simple configuration, the broad range of combustion conditions, and the high quality experimental database, the three flames considered are well appropriate to investigate the performance of PDF methods for premixed turbulent combustion.

The three flames are generated with the same burner. Table 1 presents the mean nozzle exit velocities, the corresponding Reynolds numbers, and the centerline turbulent kinetic energy values. The burner design is shown schemat-

Table 1: Global operating characteristics of the F1, F2, and F3 flames (Chen et al., 1996). The Reynolds number Re is calculated on the basis of the nozzle diameter $D = 12mm$ and bulk velocity U_0. k_0 denotes the centerline turbulent kinetic energy at the nozzle exit.

Flame	F1	F2	F3
Equivalence ratio	1.0	1.0	1.0
Reynolds number	52500	40300	24200
U_0 $[m/s]$	65	50	30
k_0 $[m^2/s^2]$	12.7	10.8	3.82

ically in figure 1. The burner consists of a nozzle with diameter $D = 12mm$ for the main stream which is surrounded by a large pilot stream to stabilize the turbulent main jet flame. The laminar pilot stream is generated by an array (1165 holes of diameter 1 mm) of small jets issued through a cooled perforated plate. Both streams have a stoichiometric methane-air mixture (equivalence ratio $\Phi = 1$). The burner is surrounded by air at rest. The outer air is entrained into the three flames at axial positions 3D-5D, changing the flame brush to non-perfectly premixed. The experimental database includes radial profiles of the mean velocity, the turbulent kinetic energy, mean and variance of the temperature, and the mean mass fractions of the major species CH_4, O_2, CO_2, H_2O and minor species CO, H_2, OH. The error in the measurements of the mean velocity is estimated to be less than 1%, and the error of the mean temperature is expected to be less than 10%. The error in the measurements of the major species is between 8% to 15%, and the error regarding the minor species is within 20% to 25%.

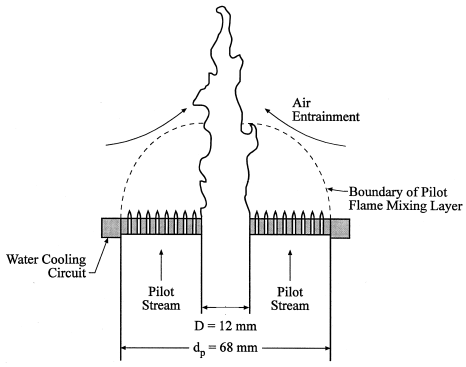

Figure 1: The burner design.

FLAME SIMULATIONS

The hybrid PDF-RANS approach was used to simulate the turbulent premixed flames described in the previous section. The evolution of the scalar PDF $F_\theta(\boldsymbol{\theta}; \boldsymbol{x}, t)$ is governed by the following transport equation, Heinz (2003):

$$\frac{\partial \langle\rho\rangle F_\theta}{\partial t} + \frac{\partial \langle\rho\rangle \overline{u}_i F_\theta}{\partial x_i} = \frac{\partial}{\partial x_i}\left[\frac{\langle\rho\rangle \overline{\nu}}{Sc_\alpha}\frac{\partial F_\theta}{\partial x_i}\right] - \langle\rho\rangle \overline{u_i^{''}|\boldsymbol{\theta}} F_\theta - \frac{\partial \langle\rho\rangle (\omega_\alpha M_\alpha + S_\alpha) F_\theta}{\partial \theta_\alpha} \quad (1)$$

where $\boldsymbol{\theta}$ denotes the sample space variable of the scalars, $\langle\rho\rangle$ denotes the ensemble averaged mass density, $\overline{\nu}$ denotes the Favre averaged molecular viscosity, Sc_α denotes the Schmidt number and a Favre decomposition $u_i = \overline{u}_i + u_i^{''}$ for velocities is used. The chemical source term S_α is treated exactly whereas closure assumptions for the conditional turbulent scalar flux $\overline{u_i^{''}|\boldsymbol{\theta}}$, the scalar mixing model M_α and the scalar mixing frequency ω_α are required. The conditional turbulent scalar flux is determined by the velocity-scalar PDF transport equation. Accordingly, the conditional turbulent flux is modeled by a gradient diffusion assumption,

$$\overline{u_i^{''}|\boldsymbol{\theta}} F_\theta = -\frac{\nu_t}{Sc_t}\frac{\partial F_\theta}{\partial x_i}. \quad (2)$$

Here, ν_t denotes the turbulent viscosity which is provided by a turbulence model, and Sc_t refers to a constant turbulent Schmidt number. The scalar mixing term M_α in the scalar PDF equation (1) was closed by adopting the IEM mixing model $M_\alpha = -(\theta_\alpha - \overline{\phi}_\alpha)$ (Dopazo and O'Brien (1974)). The standard model for the scalar mixing frequency is given by $\omega_\alpha = C_\alpha/2\tau$, where $C_\alpha = 2$ and τ denotes the time scale of the large-scale turbulent motions. It was shown by Mura et al. (2003) and Lindstedt and Vaos (2006) that the standard model for the scalar mixing frequency is not appropriate for turbulent premixed flames with fast chemistry. To overcome this problem, we developed a new model for the scalar mixing frequency based on the conservation of the scalar variance. Details on the derivation of the model can be found in Stöllinger and Heinz (2007). The equation for the scalar mixing frequency reads:

$$\omega_\alpha = -\frac{1}{2\overline{\phi_\alpha^{''2}}}\frac{\bar{D}\overline{\phi_\alpha^{''2}}}{\bar{D}t} + \frac{\nu_t}{Sc_t\overline{\phi_\alpha^{''2}}}\frac{\partial\overline{\phi}_\alpha}{\partial x_k}\frac{\partial\overline{\phi}_\alpha}{\partial x_k} + \frac{1}{2\overline{\phi_\alpha^{''2}}}\frac{\partial}{\partial x_k}\left(\frac{\nu_t + \overline{\nu}}{Sc_t}\frac{\partial\overline{\phi_\alpha^{''2}}}{\partial x_k}\right) + \frac{\overline{S_\alpha^{''}\phi_\alpha^{''}}}{\overline{\phi_\alpha^{''2}}}, \quad (3)$$

where $\bar{D}/\bar{D}t = \partial/\partial t + \overline{u}_k\,\partial/\partial x_k$ refers to the mean Lagrangian time derivative. The model for the scalar mixing frequency (3), will further be referred to as variance conserving (VC) frequency model. By adopting these closures for the conditional turbulent scalar flux $\overline{u_i^{''}|\boldsymbol{\theta}}$, the scalar mixing model M_α and the VC model for the scalar mixing frequency, the scalar PDF transport equation was solved in conjunction with RANS equations for the mean conservation of mass, momentum and energy. The realizable $k-\varepsilon$ turbulence model of Shih et al. (1995) was applied to provide the turbulent kinetic energy and characteristic frequency $1/\tau$ of large-scale turbulent motions.

The scalar PDF transport equation was solved numerically by Monte Carlo simulation. The corresponding equations for particle positions x_i^* and compositions ϕ_α^* are given by (Heinz, 2003)

$$\frac{dx_i^*}{dt} = \overline{u}_i + \frac{1}{\langle\rho\rangle Sc_t}\frac{\partial\langle\rho\rangle(\nu_t + \overline{\nu})}{\partial x_i} + \sqrt{\frac{2(\nu_t + \overline{\nu})}{Sc_t}}\frac{dW_i}{dt}, \quad (4)$$

$$\frac{d\phi_\alpha^*}{dt} = -\omega_\alpha(\phi_\alpha^* - \overline{\phi}_\alpha) + S_\alpha(\boldsymbol{\phi}). \quad (5)$$

dW_i/dt denotes the derivative of the i^{th} component of a vectorial Wiener process. The Gaussian process dW_i/dt is fully determined by its first two moments:

$$\frac{dW_k}{dt} = 0, \quad \left\langle \frac{dW_k(t)}{dt}\frac{dW_l(t')}{dt} \right\rangle = \delta_{kl}\delta(t - t'). \quad (6)$$

Here, δ_{kl} is the Kronecker delta and $\delta(t-t')$ is the delta function. The scalar mixing frequency is calculated according to

(3) for the fuel (CH_4) mass fraction because combustion takes place only if fuel is available. The equations are solved numerically by a mid-point rule in order to achieve second order accuracy in time. The time step is determined from a local time stepping procedure (Muradoglu and Pope, 2002). Averages of scalar quantities are calculated by a weighted summation over particles in a cell. For example, the term $\overline{S''_\alpha \phi''_\alpha}$ is calculated by a summation $\sum_{i=1}^{N_p} S_\alpha(\boldsymbol{\phi}^{*i})(\phi_\alpha^{*i} - \overline{\phi}_\alpha)$ over all N_p particles in a cell. The number of particles per cell is set to 80. A higher number of particles per cell was found to have no effect on simulation results. The statistical error is further reduced by averaging over the last 100 iterations. The RANS equations were solved by a second order upwind method. All computations presented have been performed by using the finite volume FLUENT code.

The chemical reaction rates $S_\alpha(\boldsymbol{\phi})$ are provided by a skeletal chemical mechanism DRM22 (Kazakov and Frenklach, 2000) consisting of 23 species (H_2, H, O, O_2, OH, H_2O, HO_2, H_2O_2, CH_2, $CH_2(S)$, CH_3, CH_4, CO, CO_2, HCO, CH_2O, CH_3O, C_2H_2, C_2H_3, C_2H_4, C_2H_5, C_2H_6, N_2) and 104 elemental reaction. The suitability of the DRM22 mechanism will be demonstrated in the next section by comparisons with results obtained with the full GRI-2.11 mechanism (Smith et al., 2000). The composition change due to chemical reactions is treated by the *in situ* adaptive tabulation (ISAT) method developed by Pope (1997).

The equations were solved on a 2-dimensional axisymmetric domain. The domain extends up to $20D$ downstream (axial direction) from the nozzle exit plane and $6.5D$ in radial direction to allow entrainment of the ambient air. The domain is discretized into 220×70 (axial by radial) cells. The grid is non-uniform to improve the accuracy of computations in the flame region. The grid independence of the solution has been checked by comparison with results obtained on a 260×100 grid.

The inlet profiles for the axial velocity and turbulent kinetic energy at the jet inlet have been taken from the experimental database of Chen et al. (1996). The profile for the turbulent dissipation rate has been calculated from the profile of the turbulent kinetic energy and measurements of the lateral length scale l_{lat} by adopting the relation $\varepsilon = \sqrt{2k/3}/l_{lat}$. The pilot composition was calculated from the chemical equilibrium of a stoichiometric methane-air mixture with 20% heat loss.

To reduce the computational time, the simulations were performed in two steps. First, a laminar flame model (see FLUENT (2006)) was used to generate realistic initial conditions for PDF simulations. The PDF simulations were then initialized with the results from the laminar flame model. Such a use of realistic initial conditions increases significantly the convergence rate of the PDF simulations. The computations have been performed parallel on four 2.8GHz Opteron processors each equipped with 4GB of SDRAM. The computational time required for a converged solution (involving approximately 30 000 iteration steps) was about 15 hours.

SIMULATION RESULTS

Radial profiles of the normalized mean axial velocity U/U_0 are presented in figure 2 at different axial positions $h = x/D$. The mean axial velocity $U = \overline{u}_1$ is normalized by the bulk velocity $U_0 = 30, 50, 65\, m/s$ for the F3, F2, and F1 flames, respectively. The overall agreement between simulation results and measurements is excellent. The thermal expansion within the turbulent jet can be recognized by the

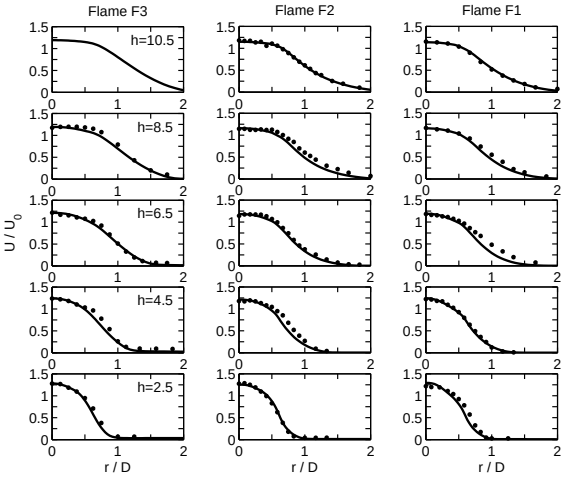

Figure 2: Normalized mean axial velocities U/U_0 for the F3, F2, and F1 flames. Dots denote experimental results of Chen et al. (1996), and lines denote simulation results.

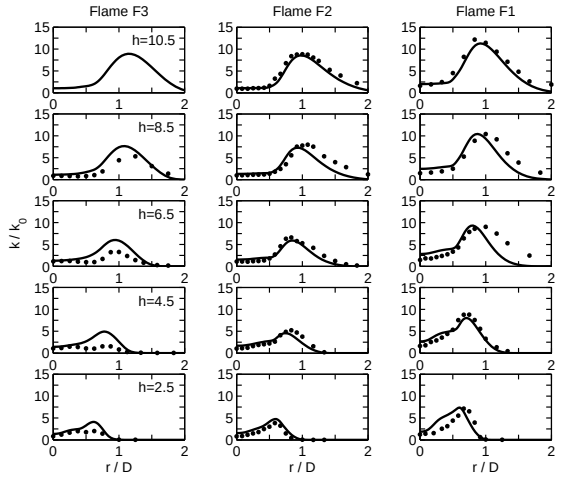

Figure 3: Normalized turbulent kinetic energy k/k_0 for the F3, F2, and F1 flames. Dots denote experimental results of Chen et al. (1996), and lines denote simulation results.

increase of the axial velocity at radial positions $r/D > 0.5$ along the x-axis for all three flames. As a result of this expansion, the shear layer (which is roughly located at the position of the maximum gradient of the mean axial velocity) is pushed outward in radial direction. This trend can also be seen in figure 3 where radial profiles of the normalized turbulent kinetic energy k/k_0 ($k_0 = 3.82, 10.8, 12.7\, m^2/s^2$ for the F3, F2, and F1 flames, respectively) are shown. The peaks of the turbulent kinetic energy k are shifted outward for increasing axial positions. The results for the higher Reynolds number F2 and F1 flames agree very well with the measurements whereas an overprediction of the turbulent kinetic energy can be seen regarding the F3 flame, especially close to the burner head. Similar overpredictions have been reported by Lindstedt and Vaos (2006). The F3 flame was also studied by Pitsch and De Lageneste (2002) by using LES in combination with a level set approach. Their turbulent kinetic energy results show a better agreement at $h = 2.5$ but a similar disagreement at $h = 6.5$. The F3 flame has the lowest axial velocity and the highest temperature. Thus, low Reynolds number effects which are not accounted for in the $k - \varepsilon$ model applied may be the reason for the turbulent

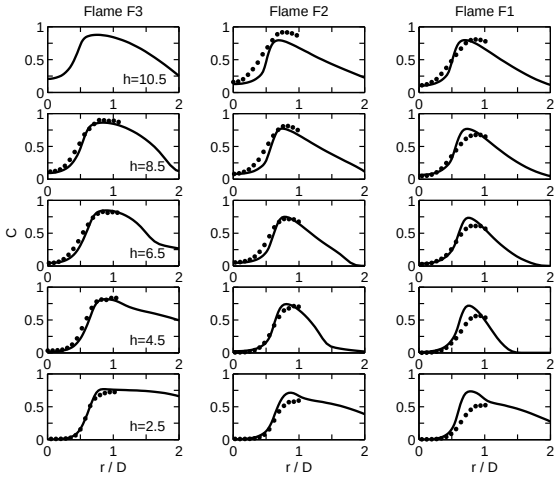

Figure 4: Mean reaction progress variable C for the F3, F2, and F1 flames. Dots denote experimental results of Chen et al. (1996), and lines denote simulation results.

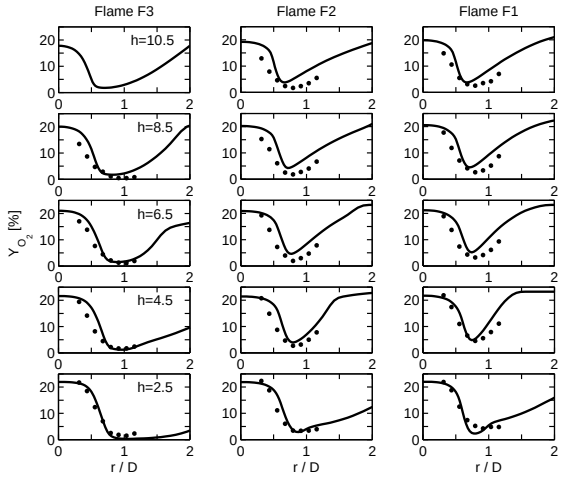

Figure 5: Mean O_2 mass fraction Y_{O_2} in percent for the F3, F2, and F1 flames. Dots denote experimental results of Chen et al. (1996), and lines denote simulation results.

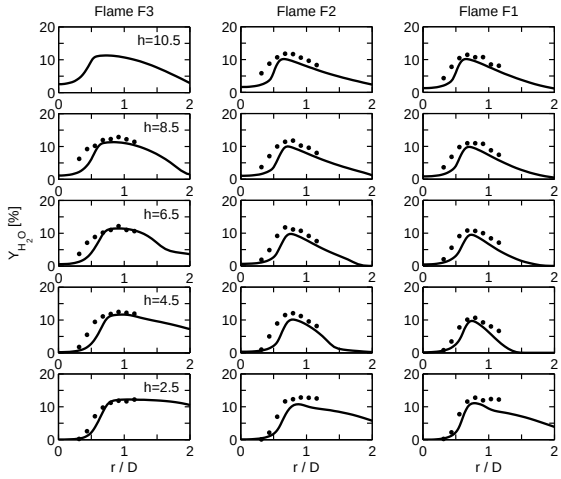

Figure 6: Mean H_2O mass fraction Y_{H_2O} in percent for the F3, F2, and F1 flames. Dots denote experimental results of Chen et al. (1996), and lines denote simulation results.

kinetic energy overprediction.

Figure 4 shows radial profiles of the mean reaction progress variable $C = \overline{T} - T_u/(T_b - T_u)$ at different axial positions for the three flames considered. Here, $\overline{T}$ is the mean temperature, $T_b = 2248\,K$ is the adiabatic flame temperature and $T_u = 298\,K$ is the temperature of the surrounding air. The simulation results of the F3 flame agree very well with the measurements. This agreement indicates that the new VC frequency model is well applicable to flamelet conditions. The F2 and F1 flame simulation results show an overprediction of the progress variable at $h = 2.5$. Lindstedt and Vaos (2006) found a similar overprediction in their F1 flame simulations using the same pilot inlet conditions. A reason for the observed overprediction of the temperature close to the burner exit regarding the F2 and F1 flames could be given by the complex interaction between the turbulent jet and laminar pilot stream. Such flow conditions are rather difficult to predict within the RANS framework. LES results for the F2 and F1 flames could clarify whether this is indeed the reason for the observed overprediction. However, such LES results have not been reported so far. Possibly, a better agreement between simulation results and measurements may be obtained by adopting refined inlet conditions (e.g., a reduction of the pilot inlet temperature regarding the F2 and F1 flames).

Figure 5 shows simulation results of the mean oxygen mass fraction Y_{O_2}. The oxygen concentration is well predicted in all three flames. The entrainment of surrounding air is clearly visible in figure 5. It is most intense in the highest Reynolds number F1 flame due to the high turbulence intensity. Mean mass fractions of the product species Y_{H_2O} and Y_{CO_2} are shown in figures 6 and 7, respectively. The H_2O concentration results agree very well with the measurements for all three flames. The CO_2 concentration of the F3 flame is also well predicted whereas the F2 and F1 flame results display a slight CO_2 underprediction. Figure 8 presents radial profiles of the mean CO mass fraction Y_{CO}. This figure shows for all three flames a significant overprediction of CO which increases downstream. This finding could explain the underprediction of the CO_2 concentration in the F2 and F1 flames: the slightly too high temperature levels in the F2 and F1 flame simulations imply high CO levels and a corresponding slower oxidation of CO to CO_2. The CO overestimation in the F3 flame cannot be explained in such a way since the temperature and CO_2 levels are well predicted. Similar high CO levels have been reported by Lindstedt and Vaos (2006). The estimated error in the measurements of Chen et al. (1996) regarding the minor species CO and OH is between 20% and 25%. Thus, the errors of measurements cannot explain the overpredictions of up to 100% which are observed in the simulations. Simulations with the full GRI 2.11 mechanism do not improve the CO predictions (see the discussion of the influence of differently complex chemical mechanisms in the following paragraph). Given the relatively well predictions of all the other species it is unclear which reason may cause the observed discrepancy between CO measurements and simulation results.

The influence of differently complex chemical mechanisms and finite-rate chemistry effects on the predictions of transported PDF methods have been studied in previous investigations, see for example Masri et al. (2004) and Lindstedt et al. (2004). Two different chemical mechanisms have been applied here to study the influence of the chemistry scheme: simulation results obtained with the DRM22 skeletal mechanism are compared in figure 9 with results obtained with the full GRI 2.11 mechanism. CO and OH

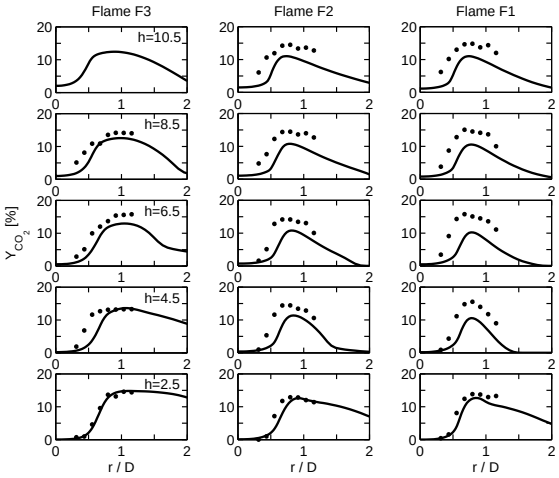

Figure 7: Mean CO_2 mass fraction Y_{CO_2} in percent for the F3, F2, and F1 flames. Dots denote experimental results of Chen et al. (1996), and lines denote simulation results.

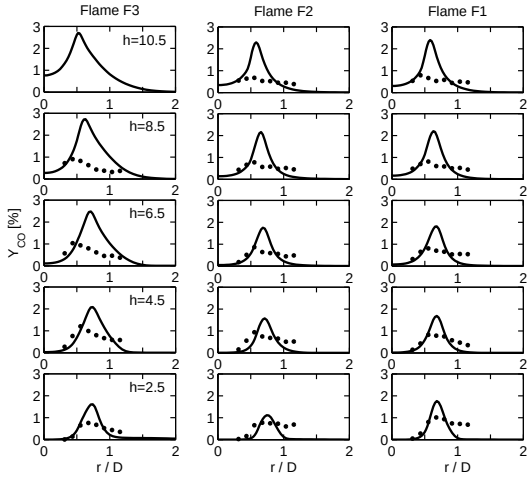

Figure 8: Mean CO mass fraction Y_{CO} in percent for the F3, F2, and F1 flames. Dots denote experimental results of Chen et al. (1996), and lines denote simulation results.

mass fractions of F3 flame simulations are shown to address the overestimation of CO predictions and sensitivity of the OH-radical concentration. In both F3 flame simulations, the IEM mixing model was used in combination with a constant $C_\alpha = 6$ value. One observes that the results obtained with the different mechanisms are almost identical. This fact indicates that the simplifications used to obtain the skeletal mechanism DRM22 do not affect the simulation results.

To investigate the influence of the mixing model M_α, simulations of the three flames considered have been performed by adopting the CD (Janicka et al., 1979) and IEM (Dopazo and O'Brien, 1974) mixing models. The scalar mixing frequency was provided by the VC frequency model. Figure 10 shows F1 flame simulation results of the mean reaction progress variable and the mean H_2O mass fraction obtained with the two mixing models in comparison to measurements. This figure shows that there is hardly any difference in the results obtained with the two mixing models. The results for the F2 and F3 flames (not shown) display an even closer agreement between the results obtained with the two mixing models. The latter fact seems to indicate a limited influence of the scalar mixing model for premixed

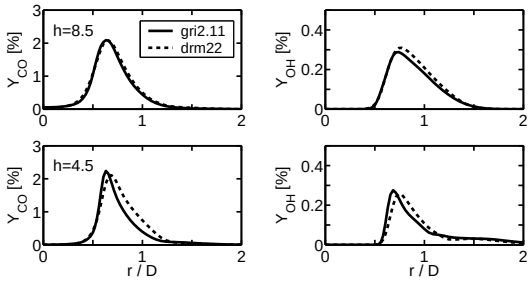

Figure 9: Comparison of simulation results for the F3 flame obtained with the GRI 2.11 mechanism (solid line) and the skeletal DRM22 mechanism (dashed line). The left column shows the CO mass fraction, and the right column shows the OH mass fraction. The IEM model combined with $C_\alpha = 6$ was used in both simulations.

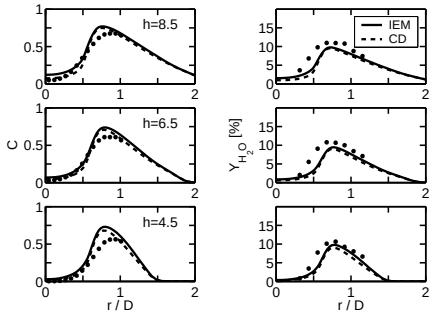

Figure 10: Simulation results for the F1 flame obtained with the CD mixing model (dashed line) and IEM (solid line) model in comparison with experimental results (dots). The left column shows the reaction progress variable C, and the right column shows the mean H_2O mass fraction.

combustion in the distributed reaction zone regime if the scalar mixing frequency is provided accurately. With regard to non-premixed turbulent combustion simulations it was found that the choice of the scalar mixing model may significantly influence the simulation results (Merci et al., 2006). However, these results were found to be very sensitive to the ad hoc choices made for C_α. It is therefore difficult to assess the influence of the mixing model separately from the mixing frequency model.

CONCLUSIONS

A review of existing PDF methods for premixed turbulent combustion shows the need for the development of a more general methodology for the explanation of scalar mixing frequencies. This problem was addressed by the introduction of the VC frequency model that conserves scalar variances. The VC model has significant conceptual advantages compared to existing methods: it is not based on empirical assumptions, there is no need to adjust several model parameters to the flow considered, and effects of chemical reactions on scalar mixing frequencies are involved without making assumptions that have an uncertain range of applicability. The computational effort required to take advantage of the VC frequency model is reasonable. Compared to the standard model for the scalar mixing frequency the increase of computational costs is given by a factor of about 1.4. The suitability of the VC scalar frequency model was demonstrated by applications to several turbulent premixed Bunsen flames that cover various regimes rang-

ing from flamelet to distributed combustion. Comparisons with existing scalar frequency models for premixed turbulent combustion made in Stöllinger and Heinz (2007) reveal the advantages of the VC frequency model. The main reason for these advantages is the following one. Existing scalar frequency models are constructed on the basis of the idea to implement chemical reaction effects explicitly in equations for non-reacting scalars. However, the investigations reported in Stöllinger and Heinz (2007) show that chemical reactions have, first of all, an implicit effect on the scalar mixing frequency: a relatively small flame thickness due to fast flamelet chemistry implies significant scalar variance gradients. The VC frequency model that conserves scalar variances then relates the relatively small flame thickness to a relatively small scalar mixing time scale (a relatively high scalar frequency) via the increase of scalar variance gradients. This important effect is correctly represented in the VC frequency model which explains its success.

ACKNOWLEDGMENTS

This work has been supported by the German Research Foundation (DFG) and Fluent Inc. (DFG Transfer Project 42). In particular, we are very thankful to Dr. M. Braun (Fluent Germany) and Professor R. Friedrich for significant support regarding the realization of this project. The authors gratefully acknowledge valuable support of Dr. G. Goldin (Fluent USA) regarding the realization of computations. The computational resources have been provided by the Institute of Scientific Computation (ISC) at the University of Wyoming.

*

References

Anand, M. and S. Pope (1987). Calculations of premixed turbulent flames by PDF methods. *Combustion and Flame 67*(2), 127–142.

Cha, C. M. and P. Trouillet (2003). A model for the mixing time scale of a turbulent reacting scalar. *Physics of Fluids 15*(9), 1375–1380.

Chen, Y., N. Peters, G. Schneemann, N. Wruck, U. Renz, and M. Mansour (1996). The detailed flame structure of highly stretched turbulent premixed methane-air flames. *Combustion and Flame 107*(3), 223–244.

Colucci, P., F. Jaberi, P. Givi, and S. Pope (1998). Filtered density function for large eddy simulation of turbulent reacting flows. *Physics of Fluids 10*(2), 499–515.

Dopazo, C. and E. O'Brien (1974). An approach to autoignition of a turbulent mixture. *Acta Astronautica 1*(9-10), 1239–1266.

FLUENT (2006). *6.3 User Guide*. Lebanon, NH: FLUENT INC.

Fox, R. (2003). *Computational Models for Turbulent Reacting Flows*. Cambridge, UK: Cambridge University Press.

Heinz, S. (2003). *Statistical Mechanics of Turbulent Flows*. Berlin: Springer-Verlag.

Janicka, J., W. Kolbe, and W. Kollmann (1979). Closure of the transport-equation for the probability density function of turbulent scalar fields. *Journal of Non-Equilibrium Thermodynamics 4*(1), 47–66.

Kazakov, A. and M. Frenklach (2000). DRM22. www.me.berkeley.edu/drm/.

Lindstedt, R., S. Louloudi, J. Driscoll, and V. Sick (2004). Finite rate chemistry effects in turbulent reacting flows. *Flow, Turbulence and Combustion 72*(2-4), 407–426.

Lindstedt, R. and E. Vaos (2006). Transported PDF modeling of high-Reynolds-number premixed turbulent flames. *Combustion and Flame 145*(3), 495–511.

Masri, A., R. Cao, S. Pope, and G. Goldin (2004). PDF calculations of turbulent lifted flames of H_2/N_2 fuel issuing into a vitiated co-flow. *Combustion Theory and Modeling 8*(1), 1–22.

Merci, B., B. Naud, and D. Roekaerts (2006). Interaction between chemistry and micro-mixing modeling in transported PDF simulations of turbulent non-premixed flames. *Combustion Science and Technology 179*(1-2), 153–172.

Mitarai, S., J. Riley, and G. Kosály (2005). Testing of mixing models for Monte Carlo probability density function simulations. *Physics of Fluids 17*(4), 047101/1–15.

Mura, A., F. Galzin, and R. Borghi (2003). A unified PDF-Flamelet model for turbulent premixed combustion. *Combustion Science and Technology 175*(9), 1573–1609.

Muradoglu, M. and S. Pope (2002). Local time-stepping algorithm for solving the probability density function turbulence model equations. *AIAA Journal 40*(9), 1755–1763.

Pitsch, H. and L. De Lageneste (2002). Large-eddy simulation of premixed turbulent combustion using a Level-Set approach. *Proceedings of the Combustion Institute 29*, 2001–2008.

Pope, S. (1985). PDF methods for turbulent reactive flows. *Progress in Energy and Combustion Science 11*(2), 119–192.

Pope, S. (1997). Computationally efficient implementation of combustion chemistry using a *in situ* adaptive tabulation. *Combustion Theory and Modelling 1*(1), 41–63.

Sanders, J. P. H. and I. Goekalp (1998). Scalar dissipation rate modelling in variable density turbulent axisymmetric jets and diffusion flames. *Physics of Fluids 10*(4), 938–948.

Shih, T. H., W. W. Liou, A. Shabbir, Z. Yang, and J. Zhu (1995). A new $k-\varepsilon$ eddy-viscosity model for high Reynolds number turbulent flows - Model development and validation. *Computers and Fluids 24*(3), 227–238.

Smith, G., D. Golden, and M. Frenklach (2000). Gri-mech 2.11. www.me.berkeley.edu/grimech.

Stöllinger, M. and S. Heinz (2007). PDF modeling and simulation of turbulent premixed flames. Submitted for publication.

Xu, J. and S. Pope (2000). PDF calculations of turbulent nonpremixed flames with local extinction. *Combustion and Flame 123*(3), 281–307.